Science Advances

AAAS

advances.sciencemag.org/cgi/content/full/4/5/eaar5809/DC1

Supplementary Materials for

Climate models predict increasing temperature variability in poor countries

Sebastian Bathiany, Vasilis Dakos, Marten Scheffer, Timothy M. Lenton

Published 2 May 2018, *Sci. Adv.* **4**, eaar5809 (2018)
DOI: 10.1126/sciadv.aar5809

This PDF file includes:

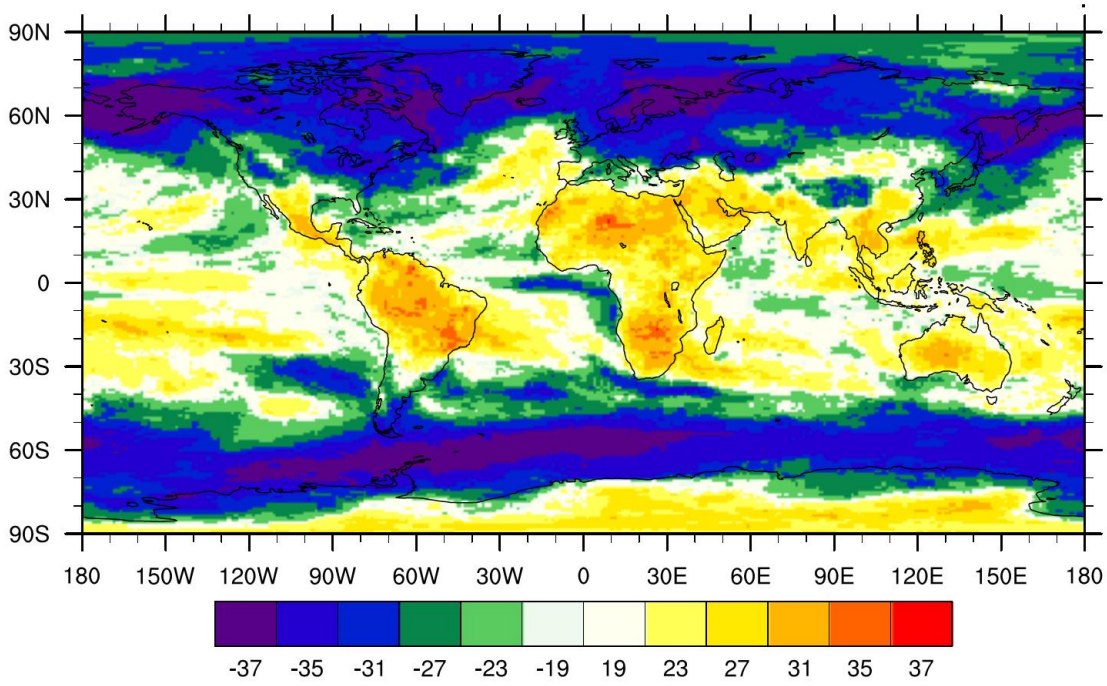

fig. S1. Model agreement on changes in SD in monthly anomalies for all months of the year. The color indicates how many of the 37 models agree on the sign of change as determined from a Kendall τ correlation (see Methods). At each grid point, the sign on the map is inherited from the majority of models, while the absolute number indicates the number of models agreeing on this specific sign.

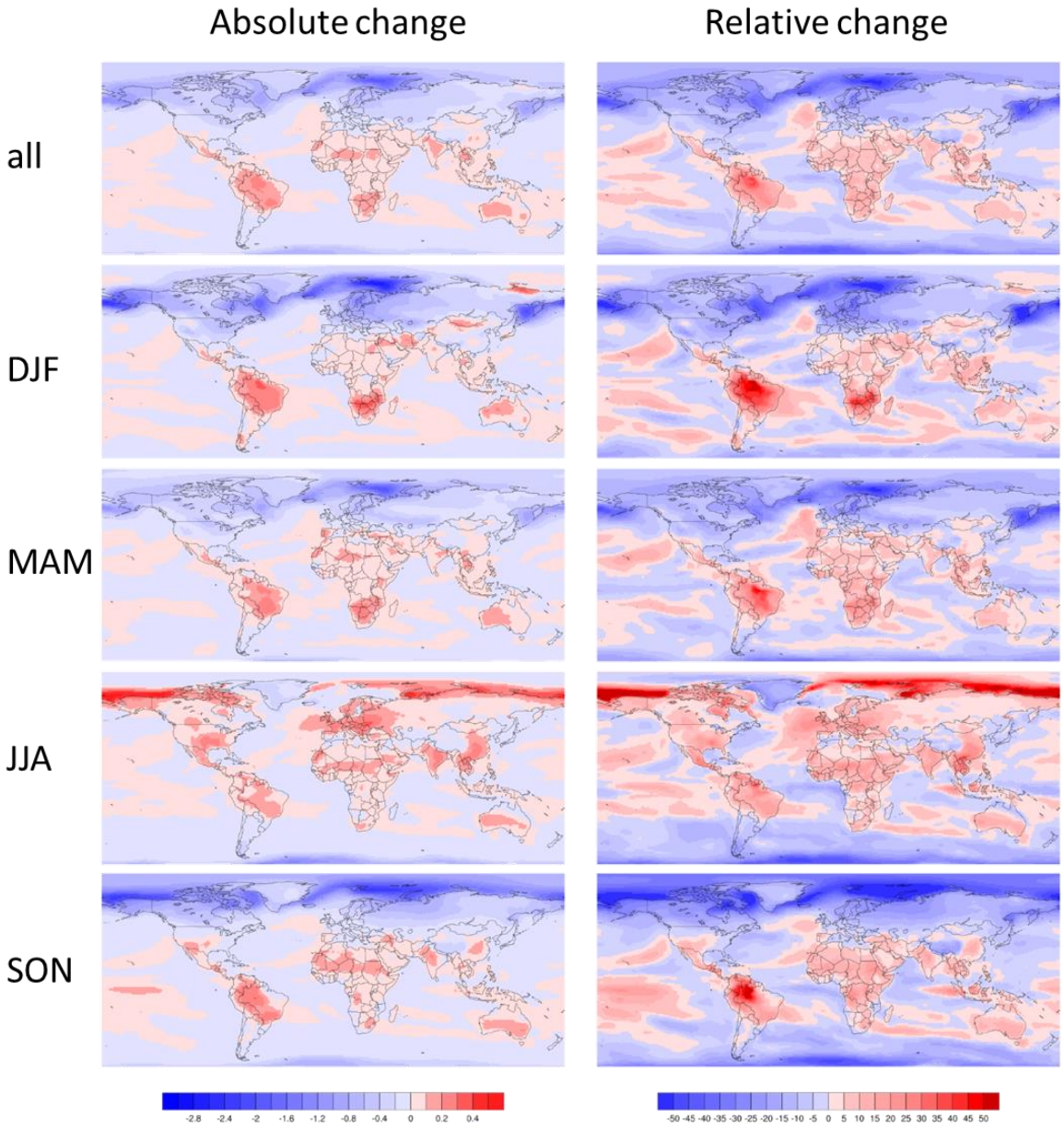

fig. S2. Absolute and relative changes in SD of monthly temperature anomalies until the end of the 21st century. The top row shows the result when using all monthly anomalies, while the other rows result from selecting anomalies from a specific season. Changes are based on the difference from 1875-1904 to 2055-2084 averaged over all 37 models. JJA: June-July-August, DJF: December-January-February, MAM: March-April-May, SON: September-October-November.

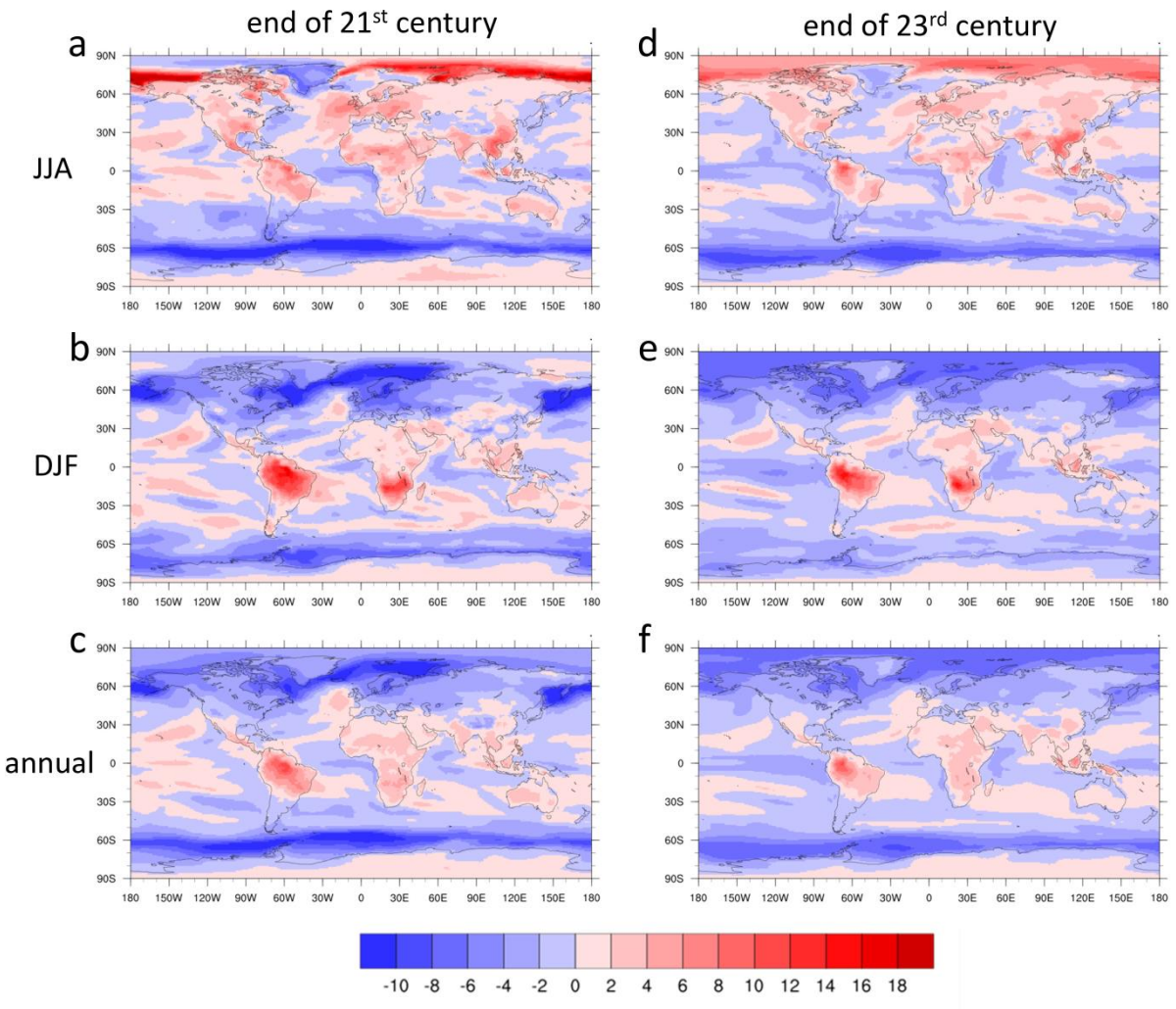

fig. S3. Relative change in SD of monthly temperature anomalies per global mean warming. Relative change in the SD of monthly temperature anomalies per global mean warming (in %/K) from 1875-1904 to 2055-2084 for all 37 models (**a**-**c**), and to 2255-2284 for the nine models run to 2300 (**d**-**f**). Temperature anomalies were selected for boreal summer (a,d), austral summer (b,e) or the whole year (c,f). JJA: June-July-August, DJF: December-January-February.

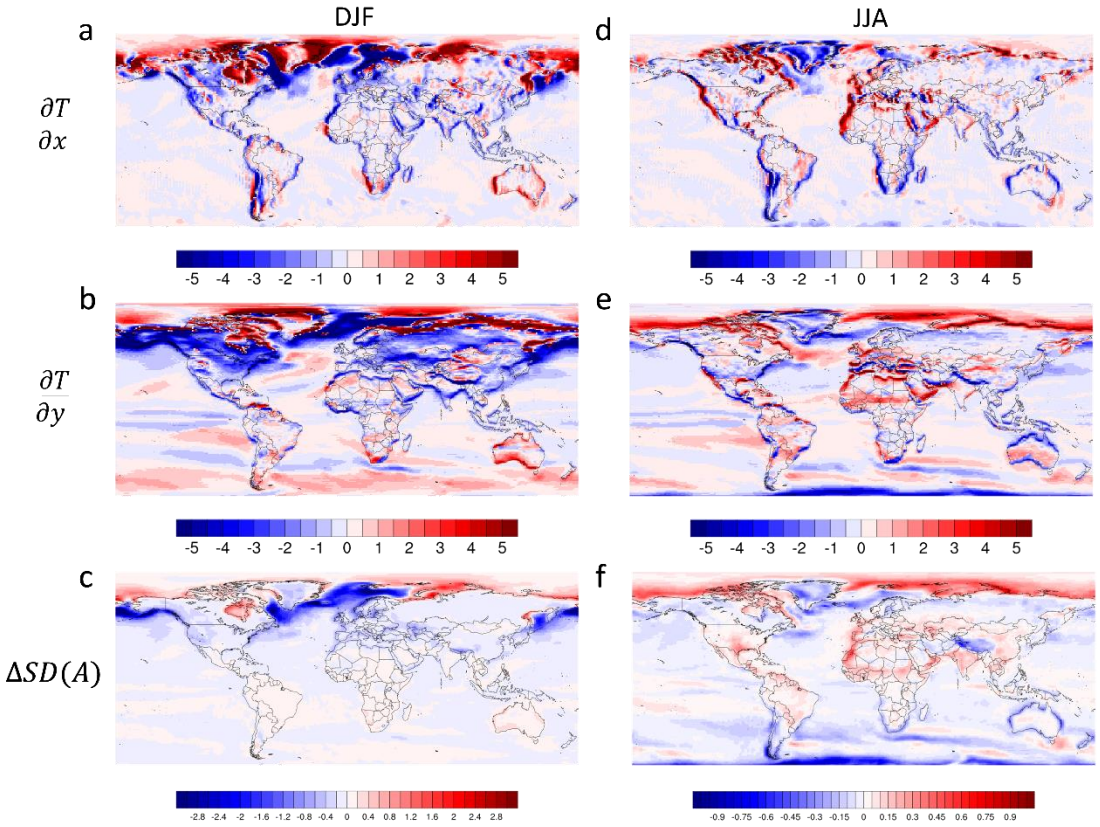

fig. S4. Changes in temperature gradients and SD due to advection. Changes in temperature gradients and SD due to advection from 1875-1904 to 2055-2084, averaged over all 37 models and austral summer (**a-c**) and boreal summer (**d-f**). The top four panels show the changes in horizontal (a,d) and meridional (b,e) gradients of the surface air temperature in K per 1000 km. The two bottom panels (c,f) show the changes in standard deviation of the temperature advection in K/day. JJA: June-July-August, DJF: December-January-February.

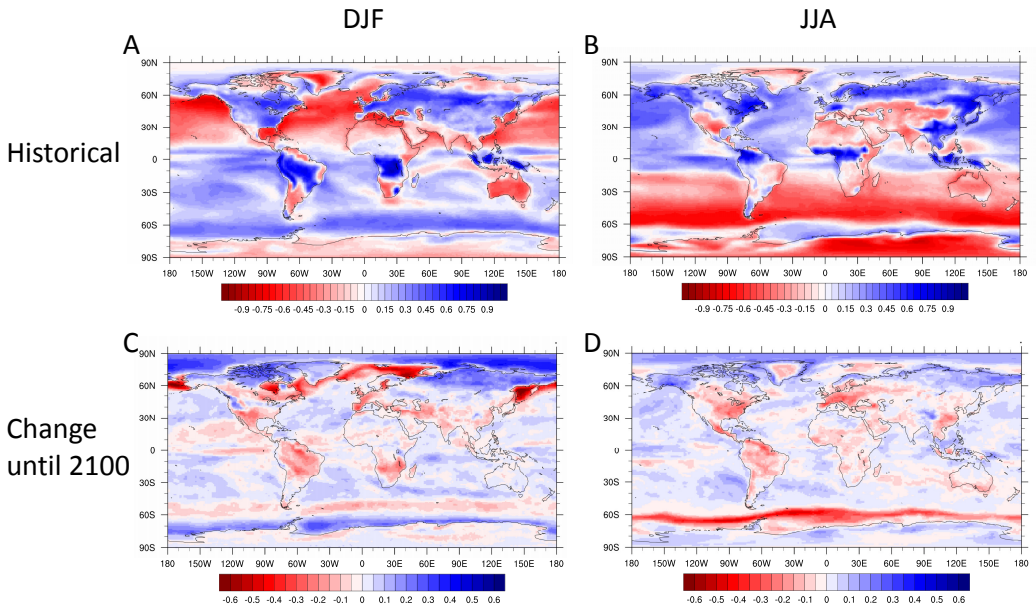

fig. S5. Temporal correlation between monthly anomalies in latent heat flux and downwelling net radiation. Temporal correlation between monthly anomalies in latent heat flux (LH) and downwelling net radiation (R_d) in the time period 1875-1904 (**a**,**b**), and the change in correlation occurring from this base period to 2055-2084 (**c**,**d**). Over land, red / blue indicates that evapotranspiration is water-limited / radiation-limited, respectively. The left two panels (a,c) show Southern hemisphere summer (DJF), the right panels (b,d) show Northern hemisphere summer (JJA).

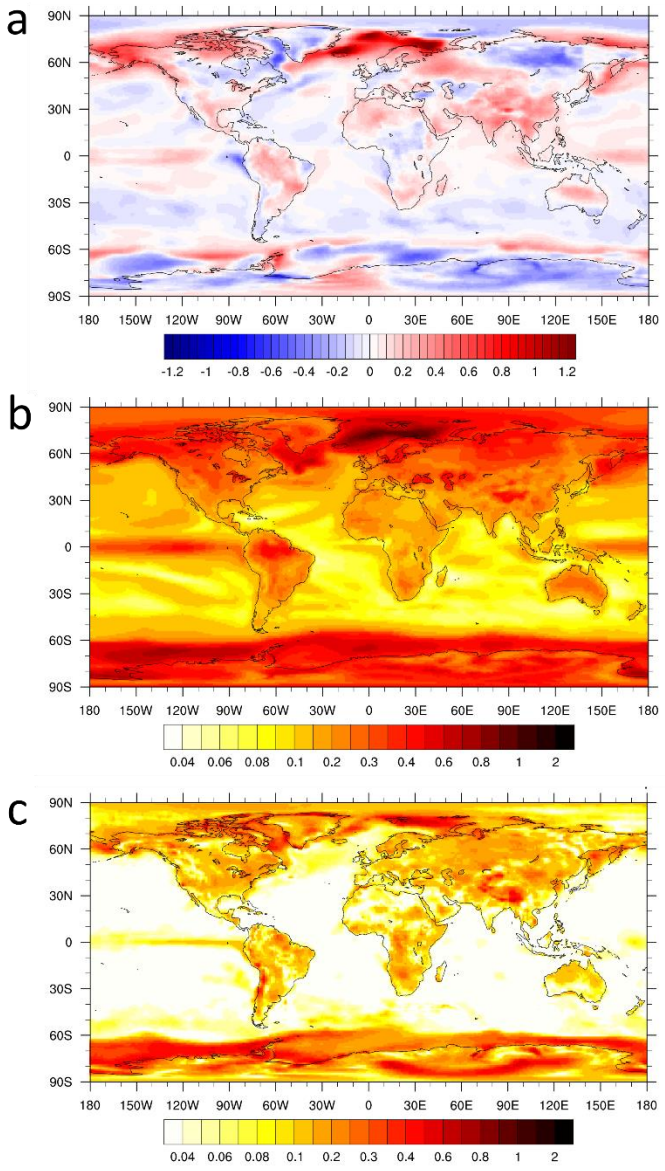

fig. S6. Model evaluation of temperature SD between 1980 and 2010. (**a**) model mean bias compared to the mean of four reanalysis datasets, (**b**) standard deviation of distribution from all 37 models, (**c**) standard deviation of distribution from all four reanalysis datasets.

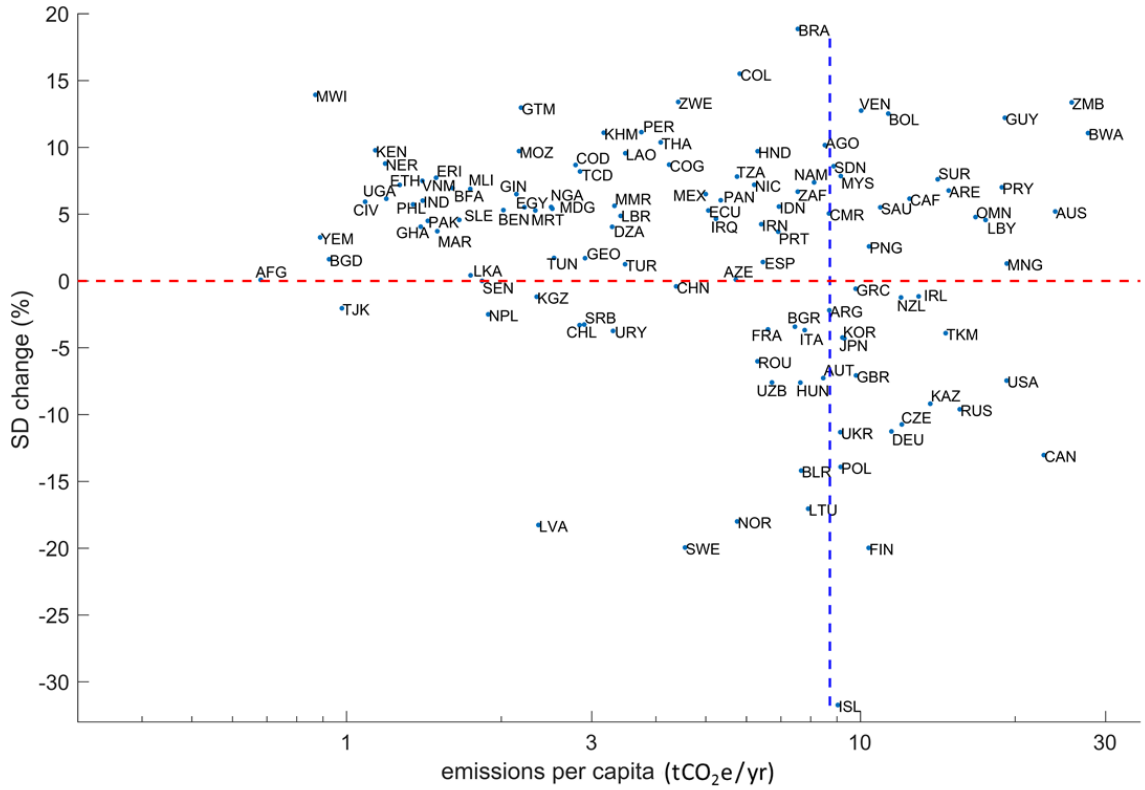

fig. S7. Greenhouse gas emissions per year and person between 1990 and 2013 versus relative change in temperature SD in different countries (using all seasons). In contrast to Fig. 5, this figure includes emissions from land use and forestry.

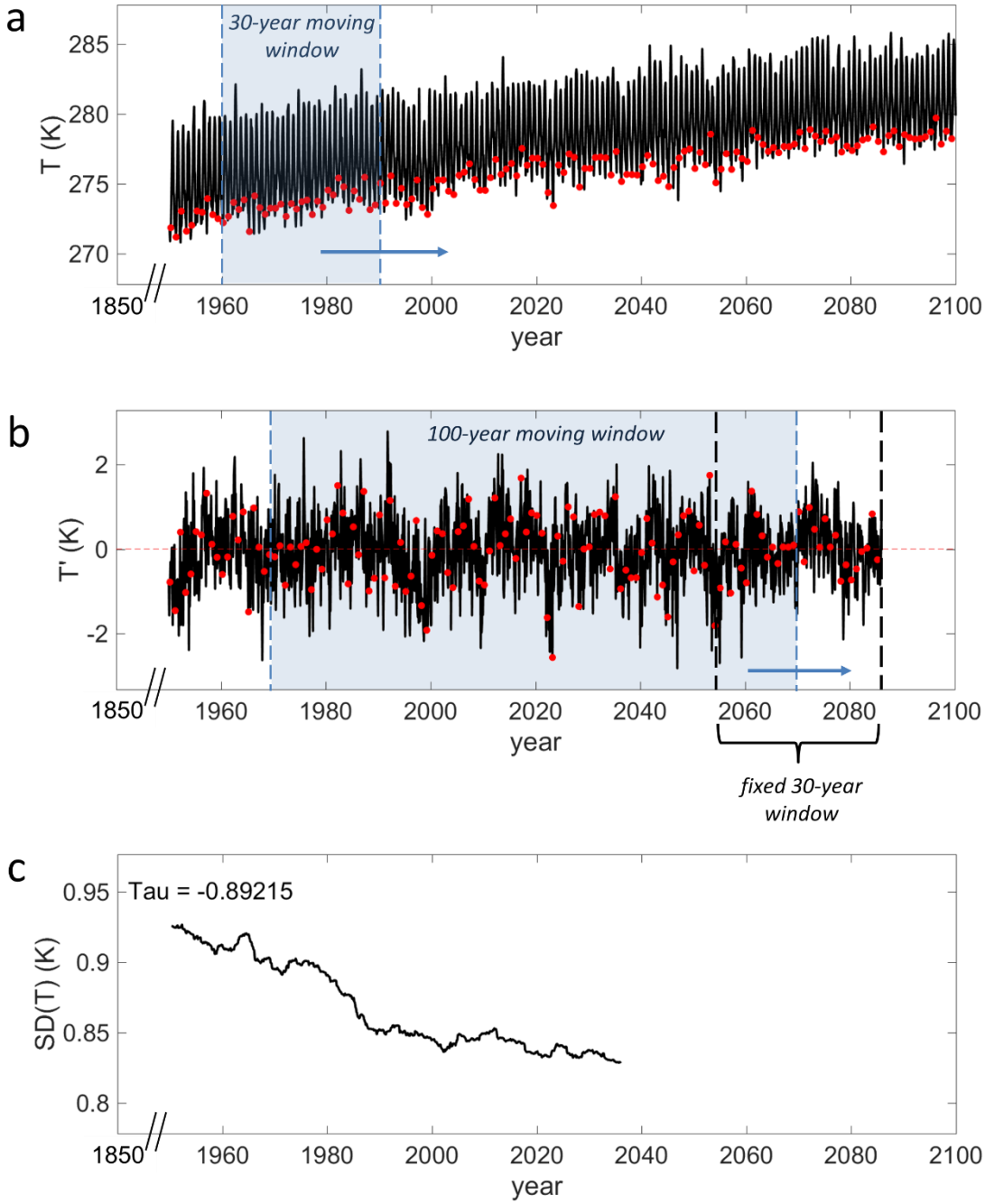

fig. S8. Documentation of our time series analysis method. (**a**) original temperature time series at a single grid cell in the North Atlantic (null meridian, 70°N) in MPI-ESM-LR. The blue window shows the 30-year sliding window used to detrend the data and remove the annual cycle. (**b**) Resulting anomaly time series. The window marked by the black dashed lines enclosing the years 2055-2084 is the time window used to calculate absolute and relative changes of temperature variability (compared to the period 1875-1904 which is not shown). The blue 100-year sliding window is used to calculate the change in standard deviation over the whole time period 1850-2100, and to calculate the Kendall τ value of the trend. (**c**) Resulting time series of standard deviation in this 100-year window, and the Kendall τ value for the entire period. This time series ends in 2035 because we are plotting at the centre of the 100-year window. Red dots in a and b mark the December of each year. The original time series starts in 1850, but only the range 1950-2100 is shown for illustration.